

NJC

Accepted Manuscript



This article can be cited before page numbers have been issued, to do this please use: K. Górski, J. Mech-Piskorz, K. Noworyta, B. Lesniewska and M. Pietraszkiewicz, *New J. Chem.*, 2018, DOI: 10.1039/C7NJ04729K.



This is an Accepted Manuscript, which has been through the Royal Society of Chemistry peer review process and has been accepted for publication.

Accepted Manuscripts are published online shortly after acceptance, before technical editing, formatting and proof reading. Using this free service, authors can make their results available to the community, in citable form, before we publish the edited article. We will replace this Accepted Manuscript with the edited and formatted Advance Article as soon as it is available.

You can find more information about Accepted Manuscripts in the [author guidelines](#).

Please note that technical editing may introduce minor changes to the text and/or graphics, which may alter content. The journal's standard [Terms & Conditions](#) and the ethical guidelines, outlined in our [author and reviewer resource centre](#), still apply. In no event shall the Royal Society of Chemistry be held responsible for any errors or omissions in this Accepted Manuscript or any consequences arising from the use of any information it contains.

Efficient Synthesis of 5-Oxatruxene and Unusual Influence of Oxygen Heteroatom on its Physico-Chemical Properties

Krzysztof Górski*^a, Justyna Mech-Piskorz*^a, Krzysztof Noworyta^a, Barbara Leśniewska^a, Marek Pietraszkiewicz^a

^a Institute of Physical Chemistry, Polish Academy of Sciences, Kasprzaka 44/52, 01-224 Warsaw, Poland. E-mail: kgorski@ichf.edu.pl, jmech@ichf.edu.pl

† Electronic supplementary information (ESI) available including synthetic procedure, ¹H, ¹³C NMR spectra, additional spectroscopic, thermal, electrochemical and calculation data.

ABSTRACT: This paper describes effective synthesis of oxatruxene and its photophysical, electrochemical and structural features that transpire when a methylene unit in a truxene core is replaced by oxygen to yield 5-oxatruxene. This modification broke C_{3h} symmetry and at the same time introduced more electronegative structure, as revealed by a four-fold increase in quantum yield, while compared to truxene. Derivatives of this material have great potential in optoelectronic devices and in organic photovoltaics. The proposed new synthetic method can be used for introducing other heteroatoms into the truxene system.

1. Introduction

Organic advanced materials gain tremendous impact on manufacturing of OLEDs (organic light emitting diodes), OFETs (organic field effect transistors) and OPVs (organic photovoltaics). The assumptions are not always fulfilled, but the effort towards simpler and lower cost production was enormous in the recent years and the stake is high.¹ Nowadays organic devices can compete with inorganic analogues in many areas like illumination, displays, radio frequency identification (RFID) tags, or solar cells. Despite many optimistic reports about organic electronics, the performance of organic materials still has to be improved. The research is continued in many directions: optimization of the position of energy levels and carrier mobility, enhancement of a quantum yield, improvement of thermal, chemical and mechanical stability and facilitating the production process.

Up to now, modified truxene structures occur in photovoltaics as: sensitizers¹⁻⁶ or hole transporting materials,⁷ in OFETs,⁸ OLEDs,⁹⁻¹⁵ as fluorescence probes,¹⁶⁻¹⁸ anticancer drugs¹⁹ and finally in non-linear optics for two photon absorption^{14,20-22} or organic lasers.²³⁻²⁶

In many cases truxenes stand as stable and compact scaffolds, with convenient spots for modification, Chart 1 a). Optimization of the position of energy levels seems to be the fundamental step in obtaining desired material. One possible way to tune the energy levels in truxenes is to incorporate different conjugated units such as oligothiophenes,²⁷ oligofluorenes,^{25,28-30} oligo(thienylethynylene)³¹, or oligo(p-phenylene).³² Other way for band-gap tuning can be achieved by the ring-fusing process in naphthalene modified truxenes.³³ Some of the modifications result in solid-state materials with pure and stable blue electrolu-

minescence. These compounds were successfully used in OLEDs and as lasing material in organic lasers.^{25,26} It seems that all possibilities of peripheral modification have been explored.³⁴⁻³⁶ However, it turned out that complicated and robust structure is not the key to obtain desirable compounds. Simple modification of the truxene unit by incorporation of heteroatom in the cyclic scaffold gives surprising results. First report about synthesis of heterocyclic truxenes was published in 1978.³⁷ Acidic trimerization of three identical subunits results in trioxa-,^{37,38} trithia-³⁹⁻⁴¹ and triazatruxenes.^{19,40,42-47} The C_{3h} symmetry of triheterotruxene is preserved, and the most visible change in new compounds is the difference in the intermolecular interaction. These compounds found their application mostly as cores of discotic liquid crystals, however they seem to be promising in organic electronic, non-linear optics and even as supercapacitors.^{48,49,50} It is much harder to introduce one, or two heteroatoms in the truxene skeleton, an example of which is 5-oxatruxene. Breaking the symmetry of the truxene basic moiety leads to expected spectral changes, very promising in OLEDs and OPV applications. However, synthetic methods used in obtaining triheterotruxenes usually fail in the case of monohetero- and diheterotruxenes. 5-Thiatruxene, recently obtained by Maciejczyk *et. al.*⁵¹ was synthesized by modification of commonly used approach in truxene chemistry. Unfortunately, this method fails when oxygen atom is introduced into the truxene core. This paper presents new, ingenious approach for obtaining 10,10,15,15-tetraethyl-5-oxatruxene, which can be successfully applied in demanding organic electronics.

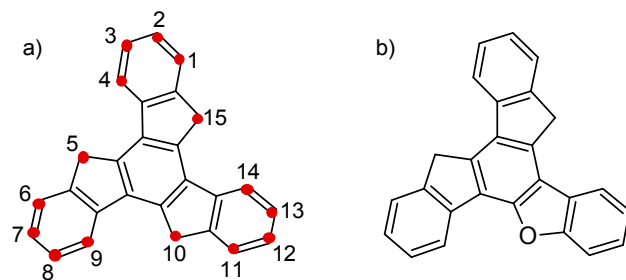


Chart 1. Structure of purely carbon truxene a) (red spots mark modification places) and 5-oxatruxene b).

2. Experimental

Absorption spectroscopy measurements were performed on UV-Vis spectrophotometers: UV-2401 and UV-2700 equipped with an integrating sphere (Shimadzu, Japan). Emission spectra were collected using a Fluorolog FL3-22 instrument with an integrating sphere (Horiba Jobin Yvon, France). Measured samples were dissolved in dichloromethane (distilled prior to the experiment), in methylcyclohexane (spectroscopic grade, Sigma-Aldrich). Solid state measurements were performed in barium sulphate (spectroscopic grade, delivered by Shimadzu). Calculations were made by using DFT theory with B3LYP/6-31g(d,p) functional and basis set for molecules in vacuum. For modelling Gaussian 09 Rev. E.01 software was used. The X-ray diffraction data were collected at X-ray diffractometer SuperNova (Agilent, UK) equipped with a CuK α micro-focus X-ray source and an Oxford Cryosystems open-flow nitrogen cryostat. Measurements were carried out at 100K. Crystal structures are deposited in the Cambridge Crystallographic Data Centre as CCDC 1526309-1526310. Thermogravimetry analysis, TGA and differential scanning calorimetry, DSC were performed with a TG-DSC 111 instrument (Setaram Instrumentation, France) under nitrogen. All electrochemical experiments were performed in a standard three-electrode electrochemical cell connected to SP-300 potentiostat/galvanostat (Bio-Logic, France) driven by EC-Lab software. Tetra-n-butylammonium hexafluorophosphate, (TBA)PF₆, electrochemical grade, decamethylferrocene, and anhydrous acetonitrile (ACN), all of Sigma-Aldrich, were used without further purification.

Platinum spiral and silver wire were used as counter and pseudo-reference electrode, respectively. Glassy carbon working electrode, 2 mm in diameter, has been used throughout all experiments. Decamethylferrocene has been used as an internal potential reference and all potentials were recalculated to its half-wave potential first, and then referred to ferrocene/ferrocenium redox couple for easier comparison with literature data. All voltammograms were recorded in 0.1 M (TBA)PF₆, ACN solutions deaerated prior to measurements by passing through it stream of argon N5.0.

3. Results and Discussion

Truxene is an aromatic compound consisting of fluorene fused with two indene moieties, Chart 1 a). 5,5,10,10,15,15-hexaethyltruxene, **CCC** has the same core with additional six out of plane ethyl groups presented at Chart 2 a). The presence of alkyl substituents significantly increases the solubility of this compound. 5-Oxatruxene is identical as truxene with one exception, fluorene is replaced by dibenzo[b,d]furan, Chart 1 b). Analogous to the previous, 10,10,15,15-tetraethyl-5-oxatruxene, **OCC** has additional four ethyl groups, Chart 2 b).

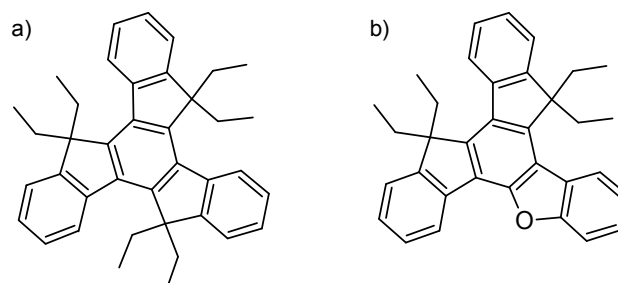


Chart 2. Structure of **CCC** a) and **OCC** b).

The role of heteroatom in the aromatic structures was examined in the case of fluorene and dibenzofuran as the basic truxene subunits. This experiments were done as a proof of concept, how the heteroatom influences quantum yield of the compound. Value of the fluorescence quantum yield of fluorene and dibenzofuran is practically the same ($\Phi = 4\%$). The difference in quantum yield is insignificant in the case of subunits but is extreme in **CCC** and **OCC** compounds.

3.1. Synthesis

Heteroaromatic compounds which contain endocyclic oxygen atom attract significant interest, due to their potential applications in organic electronics^{52,53} or as bioactive substances,⁵⁴⁻⁵⁶ thus multiple synthesis methods of such compounds have been developed. However, all they fail when it comes to the synthesis of 5-oxatruxene **9**. Due to this fact, we were forced to develop a new, effective synthetic method leading to the formation of **9**, which is essential for the development of heterotruxene-based electroemitters. A key step of proposed synthetic path was photocyclization of the corresponding precursor **7**. Quantum-mechanical calculations and visualization of LUMO orbital suggest that photocyclization may occur, Figure 1.

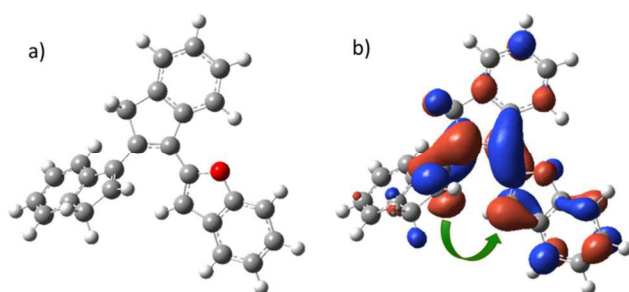
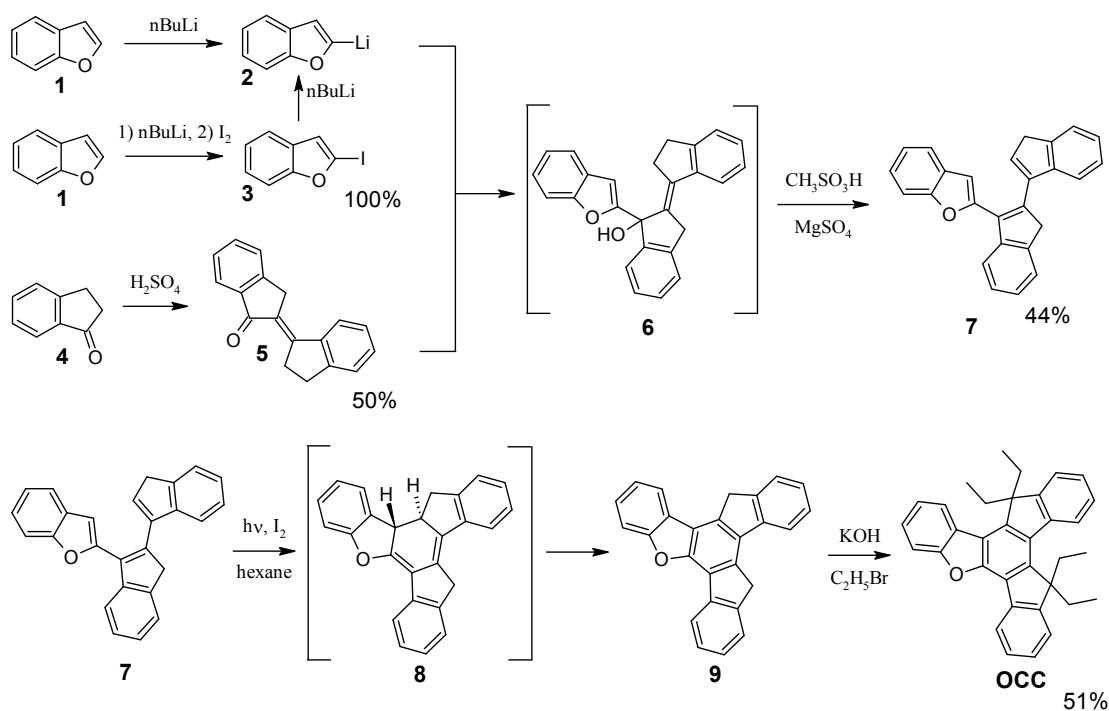
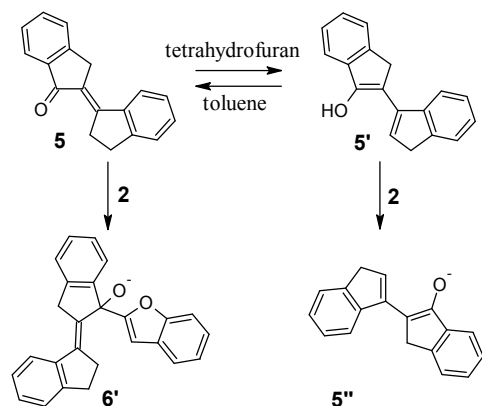


Figure 1. Structure of **7** a) and its LUMO orbital b). Arrows mark pair of corresponding electron densities participating in photocyclization.

In Scheme 1 synthetic path of **OCC** is presented. The addition of organolithium compound **2** to the corresponding ketone **5** in tetrahydrofuran did not lead to the formation of desired product **6** because of two reasons. Firstly, incomplete generation of organolithium compound **2**, secondly keto-enol tautomerism, which strongly shifts equilibrium to enol form **5'**, Scheme 2. In such conditions efficient deprotonation of compound **5'** to **5''** occurs. To favour the formation of ketone form **5**, tetrahydrofuran was replaced by toluene, but in this condition organolithium compound **2** cannot be generated efficiently by direct lithiation of benzo[*b*]furan **1**. To omit this problem, first 2-iodobenzo[*b*]furan **3** was synthesized, which after isolation was lithiated in toluene.



Scheme 1. **OCC** synthesis path.

Scheme 2. Keto-enol equilibrium of **5**.

The obtained alcohol **6**, without purification, was dehydrated to form precursor of 5-oxatruxene, **7**. During photocyclization of **7** we observed the formation of polar by-products (confirmed by TLC), which probably possessed in their structure hydroxyl or ketone groups in 10 and 15 positions of 5-oxatruxene core **9**. The last step of synthesis of soluble derivative **OCC** was four-fold ethylation of obtained system **9**. Standard condition used in alkylation of fluorene, or carbazole did not give the expected result. Due to the presence of numerous by-products, **OCC** obtained with these methods is difficult to isolate, which is directly reflected in low reaction yield. Multiple experiments confirm that the limiting factor of alkylation reaction yield is presence of oxygen in the solvents used. Truxene anions which were generated during alkylation are more prone to oxidation than corresponding fluorene or carbazole anions. The use of deaerated solvents solves this problem, allowing to obtain **OCC** with high yield (51%).

3.2. Photophysical properties and quantum chemical calculations

Absorption and emission spectra of **CCC** are presented at Figure 2. Absorption curve in dichloromethane, Figure 2 a) consists of three major peaks, with dominant at the absorption wavelength $\lambda_{\text{abs}} = 306$ nm and molar absorption coefficient $\varepsilon = 76000 \text{ dm}^3 \cdot \text{mol}^{-1} \cdot \text{cm}^{-1}$.

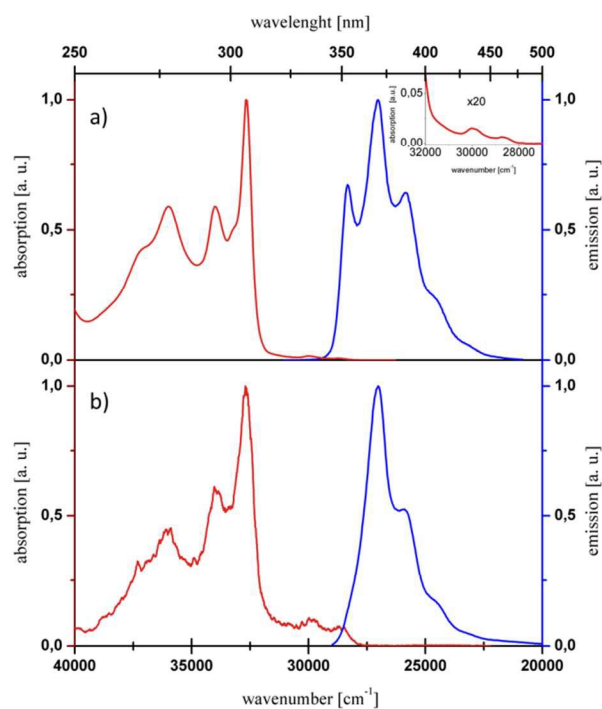


Figure 2. Normalized absorption (red) and emission (blue) spectra of **CCC** measured in dichloromethane a) and in the solid state b). Excitation in the solution: 307 nm, in the solid state: 330 nm.

The fluorescence spectrum of **CCC** in dichloromethane, shows also three well separated peaks at $\lambda_{\text{flu}} = 353, 370$ and 387 nm. Absorption and emission spectra in dichloromethane at first seems to have very large Stokes shift. However, the absorption spectrum shows also very low intensity transitions in the low energy range, where three weak bands at $348, 333$ and 318 nm are observed,

Figure 2 a) insert. These three transitions have the same energy, but relatively higher intensity in the solid state, Figure 2 b). What is more, emission shape in the solid state compared to the emission profile in dichloromethane is different. This can be result of reabsorption process of high energy peaks, which is much more efficient in dense-packed solid state structure than in solution.⁵⁷ The lack of close π - π interaction in the solid state is confirmed by no spectral shift observed between solution and solid state. Introduction of oxygen atom into the aromatic truxene system changes its photophysical properties by appearance of low energy transitions. First of all, breaking the C_{3h} symmetry in **OCC** is manifested by appearing of low energy transitions with significant intensity, Figure 3, where three well resolved peaks at 352, 337 and 322 nm are visible.

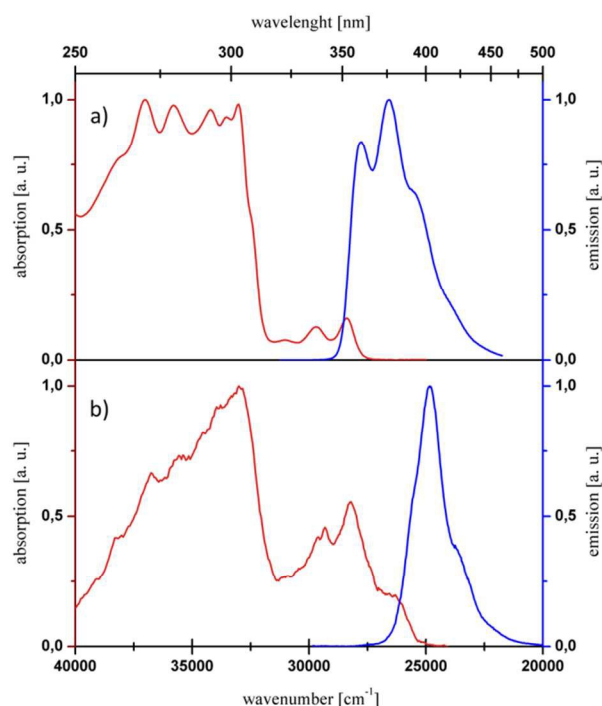


Figure 3. Normalized absorption (red) and emission (blue) spectra of **OCC** measured in dichloromethane a) and in the solid state b). Excitation in the solution: 312 nm, in the solid state: 320 nm.

Stokes shift of **OCC** spectrum in the solvent has the value 550 cm^{-1} . Interestingly, absorption spectrum has nearly constant intensity in the region 268-303 nm, with av-

erage ϵ around 30000 $\text{dm}^3\cdot\text{mol}^{-1}\cdot\text{cm}^{-1}$, Figure 3 a). **OCC** emission spectrum in the solution has similar pattern to **CCC** but at the same time is red-shifted of about 330 cm^{-1} . Absorption spectrum of **OCC** in the solid loses its nearly constant ϵ , observed in the solution. The lowest energy transitions have relatively higher intensity. The entire portion of the absorption in the solid state is clearly red-shifted in comparison to spectrum in solution by about 1500 cm^{-1} , as a result of significant π -stacking interaction of this compound in the solid state. Emission line in the solid state is distinctly different from emission in the solution because of reabsorption, which importantly decreases the intensity of the first emission peak (clear in the solution). Measured fluorescence quantum yield in the solid state is 22% and it is slightly lower than value obtained in the solution, 37%.

Table 1. Calculated vs experimental transitions of **CCC** and **OCC**.

	Transition	f_{osc}	λ_{cal} [nm]	$\lambda_{obs}^{a)}$ [nm]
CCC	$S_0 \rightarrow S_1$	0.0000	319	348
	$S_0 \rightarrow S_2$	0.0000	285	318
	$S_0 \rightarrow S_3$	0.4512	281	306
OCC	$S_0 \rightarrow S_1$	0.0540	327	352
	$S_0 \rightarrow S_2$	0.0683	294	322
	$S_0 \rightarrow S_3$	0.4507	283	303

a) measured in dichloromethane

Neglecting very low intensity bands in **CCC**, the distance between absorption and emission spectra is very large (4400 cm^{-1}), as compared with **OCC** (550 cm^{-1}). The explanation of such a behaviour is given by selection rules based on symmetry of molecules. **CCC** has C_{3h} symmetry, whereas **OCC** only C_s , what implies that in **CCC** some transitions are forbidden. Quantum-mechanical calculations supply information that in truxene first two electron transitions ($S_0 \rightarrow S_1$ and $S_0 \rightarrow S_2$), are forbidden, due to orbitals symmetry (oscillator strength, f_{osc} for these transitions equals zero), Table 1. As was mentioned before, absorption bands of corresponding transitions can be observed in the absorption spectrum of **CCC** with

very low intensities because of vibronic coupling. Breaking symmetry of the molecule due to introduction of oxygen atom in **OCC** allows transitions to S_1 and S_2 . As a consequence, additional bands in absorption spectrum (322, 337, 352 nm) can be observed. Moreover, heteroatom strongly influences radiative constant, k_r , which in dichloromethane for **CCC** is $5.00 \cdot 10^6 \text{ s}^{-1}$, whereas in **OCC** is ten times higher, $6.17 \cdot 10^7 \text{ s}^{-1}$. At the same time nonradiative constant for **CCC** is $5.06 \cdot 10^7 \text{ s}^{-1}$, whereas for **OCC** is two times higher, $1.05 \cdot 10^8 \text{ s}^{-1}$. As a result fourfold increase of **OCC** fluorescence quantum yield ($\Phi_{flu} = 37\%$) relative to **CCC** ($\Phi_{flu} = 9\%$) is observed.

In the solid state, photophysical analysis of additional nonradiative relaxation mechanisms has to be considered. For **CCC** the radiative constant practically remains

unchanged, which suggests the lack of strong intermolecular interactions. On the other hand, nonradiative constant is two times lower than in dichloromethane. The explanation of such behaviour is more rigid surrounding of every molecule in the solid state, limiting the oscillations and rotations, which as a result, increases the fluorescence quantum yield twice ($\Phi_{flu} = 19\%$). In the case of **OCC** the radiative constant increases twice, $k_r = 1.29 \cdot 10^8 \text{ s}^{-1}$, whereas k_{nr} is fourfold higher $4.59 \cdot 10^8 \text{ s}^{-1}$. Such increase of k_{nr} can be explained by the existence of an additional nonradiative channel. Crystallographic structure of **OCC** suggest the formation of excimers during irradiation which are responsible for dissipating the energy of excited state.

Table 2. Photophysical properties of **CCC** and **OCC**.

	$\lambda_{flu}^a)$ [nm]	$\Phi_{flu}^a)$ [%]	$\tau^a)$ [ns]	$k_r^a)$ [s ⁻¹]	$k_{nr}^a)$ [s ⁻¹]	$\lambda_{flu}^b)$ [nm]	$\Phi_{flu}^b)$ [%]	$\tau^b)$ [ns]	$k_r^b)$ [s ⁻¹]	$k_{nr}^b)$ [s ⁻¹]	$\lambda_{phos}^c)$ [nm]
CCC	353					-					454
	370	9	18	$5.00 \cdot 10^6$	$5.06 \cdot 10^7$	370	19	34.7	$5.48 \cdot 10^6$	$2.33 \cdot 10^7$	490
	387					385					
OCC	360					-					460
	377	37	6	$6.17 \cdot 10^7$	$1.05 \cdot 10^8$	403	22	1.7	$1.29 \cdot 10^8$	$4.59 \cdot 10^8$	497
	393					420					

a) measured in dichloromethane, b) measured in solid state, c) measured in methylcyclohexane at 77 K.

Changes of spectroscopic properties are also noticeable in emission from triplet state T_1 , Figure 4.

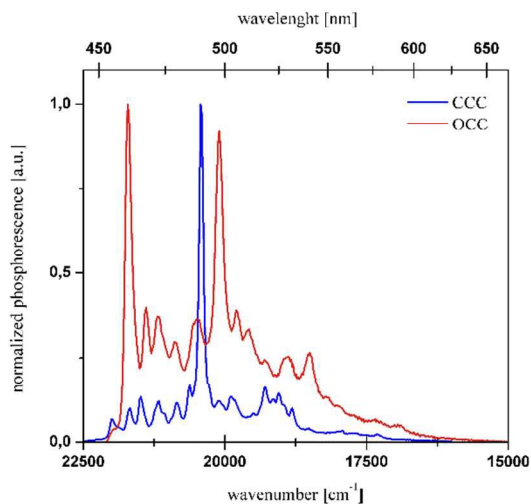


Figure 4. Phosphorescence of **CCC** and **OCC** in methylcyclohexane at 77 K. Excitation for **CCC**: 307 nm, for **OCC**: 312 nm.

In **CCC** phosphorescence spectrum, single, narrow, high intensity peak at 490 nm is present. This probably corresponds to transition from $T_1 \nu' = 0$ level to higher vibrational level of S_0 state. In **OCC** phosphorescence, two of high intensity peaks are observed, at 460 nm and 497 nm, which may correspond to transitions between $T_1 \nu' = 0 \rightarrow S_0 \nu'' = 0$ and $T_1 \nu' = 0 \rightarrow S_0$ higher vibrational level, respectively.⁵⁸

Theoretical energy diagram for truxene and 5-oxatruxene, along with corresponding molecular orbitals

are presented in Figure 5. Introduction of oxygen atom in 5-oxatruxene breaks the molecular symmetry from C_{3h} to C_s , which removes the degeneracy of the orbitals. One essential feature is a decrease in the HOMO-LUMO gap in **OCC** what is in agreement with measured UV-Vis spectra.

In **CCC** the lack of spectral shift between absorption in the solution and the solid state described above is confirmed by X-ray analysis. Six ethyl groups in **CCC** molecule effectively separates molecules from each other, which significantly hinders aggregation. Crystallographic structure gives an evidence for difficulty of stacking of **CCC** molecules, Figure 6. **CCC** crystallizes in orthorhombic, space group $Pna2_1$.

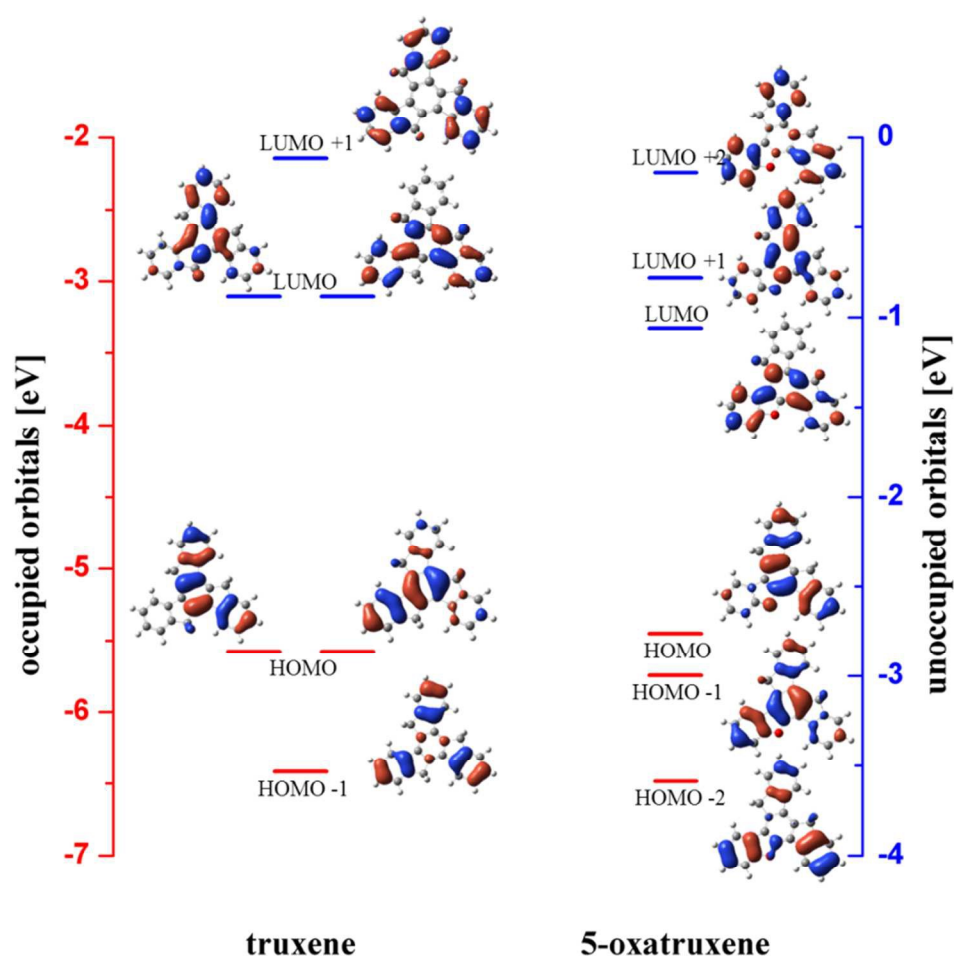


Figure 5. Calculated energy diagram of the highest occupied (red) and the lowest unoccupied (blue) orbitals of truxene and 5-oxatruxene. Molecular orbitals shapes are presented next to the energy levels.

OCC has only four ethyl groups, thus separation of molecules is more difficult, Figure 7. What is more, replace-

ment of one diethylmethylene moiety (Et_2C) by oxygen atom creates place prone to π -stacking. **OCC** crystallizes

in monoclinic, space group $P2_1/n$. Crystal structure of **OCC** consists of dimers arranged in columns from one direction, Figure 7 and herringbone pattern from another direction, Figure 8.

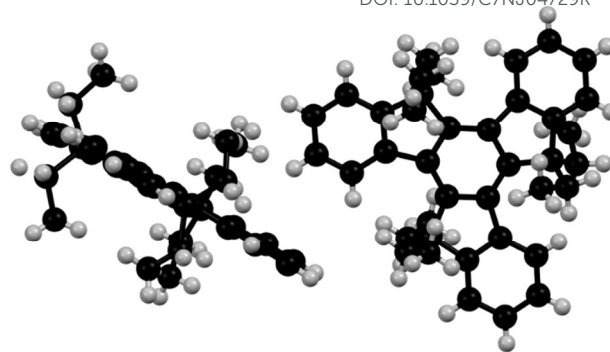


Figure 6. Crystal structure of **CCC** molecules.

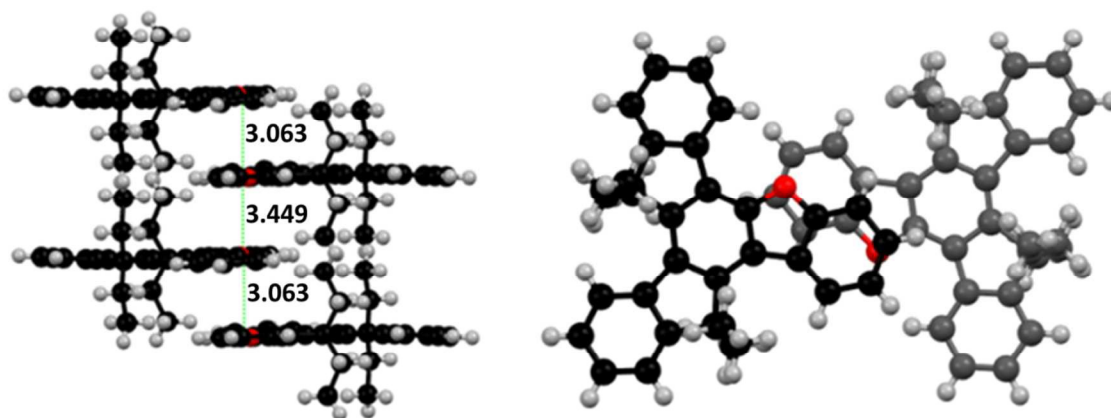


Figure 7. Crystal structure of **OCC** molecules (intermolecular distances are given in Å).

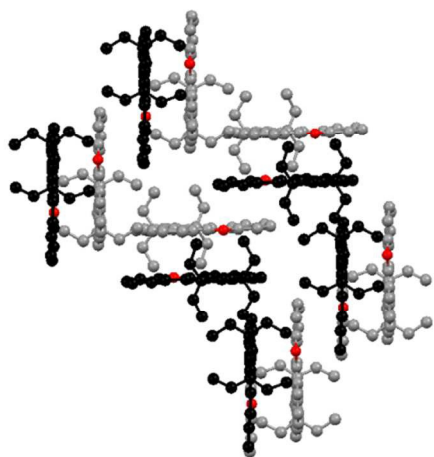


Figure 8. Herringbone orientation of **OCC** molecules.

3.3. Thermal properties

The presence of oxygen atom in the truxene core affects the thermal properties of the truxene. To investigate

them, we performed TGA and DSC analyses for **CCC** and **OCC**. Measurements were carried out in the temperature range 20-240 °C and 20-230 °C for **CCC** and **OCC** respectively, with a scan rate of 5 °C·min⁻¹, in nitrogen atmosphere. Both substances do not decompose in the examined temperatures, which confirms their high thermal stability. **CCC** has relatively broad melting peak T_m with maximum at 217.2 °C, indicating the presence of different crystalline forms (Figure S2). X-ray structure clearly shows that **CCC** crystallize with some disorder in the structure (Figure S1). Occurrence of polymorphism in truxenes is known from previous work.⁵⁹ Liquid phase of **CCC** overcools what was observed as a crystallization peak at temperature $T_{cry} = 98.7$ °C significantly lower than melting temperature, $T_m = 217.2$ °C, Table 3. No glass transition was observed in the measured system. Subsequent heating and cooling cycles reflect the same

situation. In the case of **OCC** the melting peak is much sharper, with maximum at 214.7 °C what can be interpreted as the presence of only one crystalline form (Figure S3). During cooling **OCC** undergoes glassification at $T_g = 107.8$ °C. Subsequent heating, surprisingly, reveals crystallization peak at 125.0 °C and the shift of the melting point which this time is observed at 222.4 °C. At the following cooling cycle glass transition is observed like for the first cycle at 107.8 °C. Subsequent heating-cooling cycle do not bring any changes. Increase of the **OCC** melting point in the second cycle for about 7.7 °C may suggest formation of different crystalline form. The difference in enthalpy of fusion ΔH_{fusion} in **CCC** and **OCC** of value 3.8 kJ·mol⁻¹ is caused by greater amount of energy necessary to overcome π -stacking between **OCC** molecules.

Table 3. Thermal properties of **CCC** and **OCC**.

	T_m [°C]	T_g [°C]	T_{cry} [°C]	H_{fusion} [J·g ⁻¹]
CCC	217.2	-	98.7 ^c	25.1
OCC	214.7	107.8	125.0 ^h	28.9

c - during cooling cycle, h – during heat cycle

3.4. Electrochemistry

To investigate the redox properties of **CCC** and **OCC** cyclic voltammetry was performed. During oxidation of **CCC** one quasi-reversible redox process is observed with formal potential at 1.06 V and corresponding reduction peak appears at 0.97 V (Figure S4 a)). When potential scan is extended to more positive potentials, additional irreversible oxidation process at 1.81 V occurs. The lack of corresponding reduction peak in reverse scan indicates chemical decomposition of the second oxidation product. **OCC** measured in the same potential range shows different behaviour, (Figure S4 b)). Firstly, irreversible oxidation process at 0.76 V is observed, followed by the appearance of quasi-reversible redox process at 0.96 V. In the reverse scan a small peak at 0.42 V corresponding to reduction of the first oxidation product is also observed. When reverse potential is extended to more positive

values a third, broad, oxidation peak at 1.59 V appears. It indicates irreversible process leading to formation of electrochemically inactive species as corroborated by disappearance of reduction peaks at 0.42 V and 0.93 V in the reverse scan. Differences in redox properties of **CCC** and **OCC** in positive potential range indicate strong influence of oxygen atom on formation of cation radical during oxidation. In the potential window from -0.5 to -3.4 V only one reduction peak, characteristic for irreversible process, is visible for **CCC** at -3.25 V and for **OCC** at -3.04 V, (Figure S5 a,b). Cyclic voltammograms recorded at various scan rates for **CCC** (Figure S6 a)) indicate gradual appearance of corresponding oxidation peak at -3.07 V at scan rates higher than 0.2 V·s⁻¹. This behaviour indicates relatively slow decomposition of the reduction product, and therefore, formation of relatively stable anion radical. Similar measurements performed for **OCC** (Figure S6 b)) do not show appearance of any reverse oxidation peak even at the scan rate of 5 V·s⁻¹, indicating much faster decomposition of anion radical in this case. This observation is supported by quantum mechanical calculations which show that in the case of anion radical of **CCC** negative charge is located rather in the central part of the molecule and partially on the one of peripheral benzene ring (Figure 9 a)).

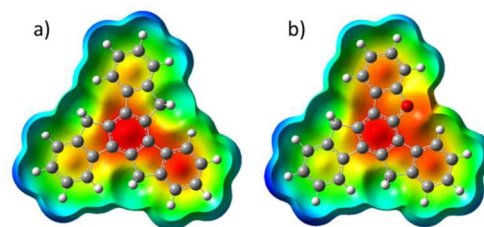


Figure 9. **CCC** a) and **OCC** b) anion radicals.

In the case of **OCC** the negative charge is additionally delocalised over benzo[b]furan moiety, (Figure 9 b)). Due to presence of the six ethyl groups, the charge is more shielded leading to the formation of more stable anion radical in **CCC** than in the case of **OCC**.

The absolute HOMO and LUMO energies can be calculated from electrochemical data according to equations 1 and 2.

$$E_{\text{HOMO}}(\text{eV}) = -e(E_{\text{ox}}(\text{V}) + 4.71 \text{ V}) \quad (1)$$

$$E_{\text{LUMO}}(\text{eV}) = -e(E_{\text{red}}(\text{V}) + 4.71 \text{ V})^{60} \quad (2)$$

Value of E_{LUMO} calculated for **OCC** is only 0.02 eV more positive than the value for **CCC**, while value of E_{HOMO} is 0.33 eV more positive for **OCC** than for **CCC**. Therefore, calculated electrochemical bandgap is slightly higher for **CCC** than for **OCC** (3.74 eV vs. 3.43 eV), which is consistent with results obtained from spectroscopic measurements, Table 5.

Table 4. Summarized redox potentials of truxene **CCC** and **OCC** in 0.1 M (TBA)PF₆, ACN solution.

	$E_{\text{ox}}(1)$ [V]*	$E_{\text{ox}}(2)$ [V]*	$E_{\text{ox}}(3)$ [V]*	E_{red} [V]*
CCC	1.06	1.81	-	-3.25
OCC	0.76	0.96	1.59	-3.04

* vs. Fc/Fc⁺

Table 5. Onset potentials and calculated HOMO, LUMO energies and band gap for truxene **CCC** and **CCO** in 0.1 M (TBA)PF₆, ACN solution.

	$E_{\text{ox}}^{\text{onset}}$ [V]*	E_{HOM} [eV]	$E_{\text{red}}^{\text{onset}}$ [V]*	E_{LUMO} [eV]	ΔE_{elc} ¹ [eV]	ΔE_{opt} ² [eV]
CCC	0.99	-5.70	-2.75	-1.96	3.74	3.55
OCC	0.66	-5.37	-2.77	-1.94	3.43	3.49

* vs. Fc/Fc⁺

¹ $\Delta E_{\text{elc}} = E_{\text{LUMO}} - E_{\text{HOMO}}$

² ΔE_{opt} determined from intersection of absorption and emission bands

4. Conclusion

Presented data reveal the changes in physical properties of the molecule as a result of the introduction of oxygen atom into truxene system. The most significant changes are seen in the photophysical properties i.e. increase of the quantum yield from 9 to 37% and appearance of low energy bands. Although the quantum yield of pure **OCC** is not record-breaking, and the redox processes are not fully reversible, ~~thus~~ the potential application of

this material in optoelectronic devices is possible, provided it will be modified.⁵² Implementation of proper donor, or acceptor moiety at the periphery of **OCC** molecule leads to donor-acceptor systems which - in general - are widely applied as emitters in OLED devices. Breaking the C_{3h} symmetry, creates non-equivalent places susceptible to selective modification. Moreover the derivatization yield is higher in the case of **OCC** than **CCC**, trioxa-, triaza- and trithatruene. In the solution **OCC** absorption spectrum, becomes nearly constant in the region 268-303 nm, with an average molar absorption coefficient around 30000 dm³·mol⁻¹·cm⁻¹, Figure 3 a). Regarding thermal properties, **OCC** has tendency for glass formation. This feature is indispensable in OLED devices fabrication. **OCC** creates a good skeleton for further modification and **OCC** derivatives have great potential in optoelectronic applications.

Replacement of diethylmethylene moiety by oxygen atom is responsible for π -stacking. In the solid state **OCC** dimers creates columns, what makes this material potentially useful as organic conductors in OFETs. **OCC** opens a new class of monoheterotruxenes which can be treated as a basic units for further modifications. Current organic optoelectronics is facing a problem with low durability of devices, thus new compounds, other than carbazole, or dibenzotriphenylene are urgently needed. The proposed synthetic plan should be applicable towards the synthesis of other heteroatom containing truxene analogues, leading to the development of a new class of truxene compounds with modulated physical properties.

CONFLICTS OF INTEREST

There are no conflicts to declare.

ACKNOWLEDGMENT

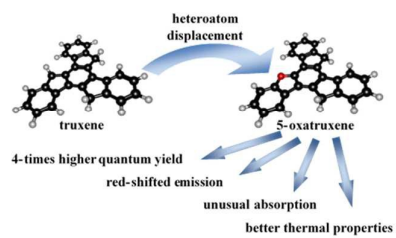
This research was supported in part by PL-Grid Infrastructure and the Institute of Physical Chemistry of the Polish Academy of Sciences. The Authors cordially thank

Professor Jacek Waluk, of the Institute of Physical Chemistry of the Polish Academy of Sciences, for his suggestions and comments concerning spectroscopic part and HOMO-LUMO calculations, and Oksana Pietraszkievicz for preparation of crystals.

REFERENCES

- (1) Z. Yang, B. Xu, J. He, L. Xue, Q. Guo, H. Xia, W. Tian, *Org. Electron.* 2009, **10**, 954–959.
- (2) X. Zong, M. Liang, T. Chen, J. Jia, L. Wang, Z. Sun, S. Xue, *Chem. Commun.* 2012, **48**, 6645–6647.
- (3) B. Du, D. Fortin, P. D. Harvey, *Inorg. Chem.* 2011, **50**, 11493–11505.
- (4) H.-J. Xu, B. Du, C. P. Gros, P. Richard, J.-M. Barbe, P. D. Harvey, *J. Porphy. Phthalocya.* 2013, **17**, 44–55.
- (5) B. Du, P. D. Harvey, *Chem. Commun.* 2012, **48**, 2671–2673.
- (6) S. Diring, R. Ziessel, *Tetrahedron Lett.* 2009, **50**, 1203–1208.
- (7) J. Wang, Y. Chen, M. Liang, G. Ge, R. Zhou, Z. Sun, S. Xue, *Dye. Pigment.* 2016, **125**, 399–406.
- (8) Y. Sun, K. Xiao, Y. Liu, J. Wang, J. Pei, G. Yu, D. Zhu, *Adv. Funct. Mater.* 2005, **15**, 818–822.
- (9) M. Kimura, S. Kuwano, Y. Sawaki, H. Fujikawa, K. Noda, Y. Taga, K. Takagi, *J. Mater. Chem.* 2005, **15**, 2393–2398.
- (10) X. Y. Cao, X. H. Zhou, H. Zi, J. Pei, *Macromolecules* 2004, **37**, 8874–8882.
- (11) W. Y. Lai, Q. Y. He, R. Zhu, Q. Q. Chen, W. Huang, *Adv. Funct. Mater.* 2008, **18**, 265–276.
- (12) J. Luo, Y. Zhou, Z.-Q. Niu, Q.-F. Zhou, Y. Ma, J. Pei, *J. Am. Chem. Soc.* 2007, **129**, 11314–11315.
- (13) M. Wu, Z. Gong, A. J. Kuehne, A. L. Kanibolotsky, Y. J. Chen, I. F. Perepichka, A. R. Mackintosh, E. Gu, P. J. Skabara, R. A. Pethrick, M. D. Dawson, *Opt. Express* 2009, **17**, 16436–16443.
- (14) L. Sanguinet, J. C. Williams, Z. Yang, R. J. Twieg, G. Mao, K. D. Singer, G. Wiggers, R. G. Petschek, *Chem. Mater.* 2006, **18**, 4259–4269.
- (15) J. Huang, B. Xu, J.-H. Su, C. H. Chen, H. Tian, *Tetrahedron* 2010, **66**, 7577–7582.
- (16) X. Du, M.-S. Yuan, F. Xu, H. Wang, Q. Wang, W. Wang, D. E. Wang, J. Wang, *Spectrochim. Acta - Part A Mol. Biomol. Spectrosc.* 2016, **164**, 33–39.
- (17) S. Gomez-Esteban, M. Pezella, A. Domingo, G. Hennrich, B. Gómez-Lor, *Chem. Eur. J.* 2013, **19**, 16080–16086.
- (18) M.-S. Yuan, Z.-Q. Liu, Q. Fang, *J. Org. Chem.* 2007, **72**, 7915–7922.
- (19) L. Ginnari-Satriani, V. Casagrande, A. Bianco, G. Ortaggi, M. A. Franceschin, *Org. Biomol. Chem.* 2009, **7**, 2513–2516.
- (20) C. K. M. Chan, C.-H. Tao, H. Tam, N. Zhu, V. W.-W. Yam, K. Cheah, *Inorg. Chem.* 2009, **48**, 2855–2864.
- (21) X. Zhou, J.-K. Feng, A.-M. Ren, *Synth. Met.* 2005, **155**, 615–617.
- (22) L. Ji, Q. Fang, M. S. Yuan, Z. Q. Liu, Y. X. Shen, H. F. Chen, *Org. Lett.* 2010, **12**, 5192–5195.
- (23) F. Goubard, F. Dumur, *RSC Adv.* 2015, **5**, 3521–3551.
- (24) G. Tsiminis, Y. Wang, P. E. Shaw, A. L. Kanibolotsky, I. F. Perepichka, M. D. Dawson, P. J. Skabara, G. A. Turnbull, I. D. W. Samuel, *Appl. Phys. Lett.* 2009, **94**, 243304–(1–3).
- (25) W.-Y. Lai, R. Xia, Q.-Y. He, P. A. Levermore, W. Huang, D. D. C. Bradley, *Adv. Mater.* 2009, **21**, 355–360.
- (26) W. Xu, J. Yi, W.-Y. Lai, L. Zhao, Q. Zhang, W. Hu, X.-W. Zhang, Y. Jiang, L. Liu, W. Huang, *Adv. Funct. Mater.* 2015, **25**, 4617–4625.
- (27) J. Pei, J. L. Wang, X. Y. Cao, X. H. Zhou, W. B. Zhang, *J. Am. Chem. Soc.* 2003, **125**, 9944–9945.
- (28) M. M. Oliva, J. Casado, J. T. L. Navarrete, R. Berridge, P. J. Skabara, A. L. Kanibolotsky, I. F. Perepichka, *J. Phys. Chem. B* 2007, **111**, 4026–4035.
- (29) K. M. Omer, A. L. Kanibolotsky, P. J. Skabara, I. F. Perepichka, A. J. Bard, *J. Phys. Chem. B* 2007, **111**, 6612–6619.
- (30) W. Zhang, X. Y. Cao, H. Zi, J. Pei, *Org. Lett.* 2005, **7**, 959–962.

- (31) J.-L. Wang, J. Luo, L.-H. Liu, Q.-F. Zhou, Y. Ma, J. Pei, *Org. Lett.* 2006, **8**, 2281–2284.
- (32) W.-B. Zhang, W.-H. Jin, X.-H. Zhou, J. Pei, *Tetrahedron* 2007, **63**, 2907–2914.
- (33) C. Cheng, Y. Jiang, C.-F. Liu, J.-D. Zhang, W.-Y. Lai, W. Huang, *Chem. Asian J.* 2016, **11**, 3589–3597
- (34) S. C. Yuan, Q. Sun, T. Lei, B. Du, Y. F. Li, J. Pei, *Tetrahedron* 2009, **65**, 4165–4172.
- (35) E. M. Pérez, B. M. Illescas, M. A. Herranz, N. Martín, *New J. Chem.* 2009, **33**, 228–234.
- (36) Y. Wu, X. Hao, J. Wu, J. Jin, X. Ba, *Macromolecules* 2010, **43**, 731–738.
- (37) J. Bergman, B. Egestad, *Tetrahedron Lett.* 1978, **19**, 3143–3146.
- (38) C. Destrade, N. H. Tinh, L. Mamlok, J. Malthete, *Mol. Cryst. Liq. Cryst.* 1984, **114**, 139–150.
- (39) J. Bergman, B. Egestad, *Tetrahedron* 1986, **42**, 763–773.
- (40) F.-W. Yen, C.-M. Teng, Luminescence Technology Corporation, US 2016/0233427 A1, 2016.
- (41) N. H. Tinh, R. Cayuela, C. Destrade, J. Malthete, *Mol. Cryst. Liq. Cryst.* 1985, **122**, 141–149.
- (42) W.-Y. Lai, R. Zhu, Q.-L. Fan, L.-T. Hou, Y. Cao, W. Huang, *Macromolecules* 2006, **39**, 3707–3709.
- (43) N. Robertson, S. Parsons, E. J. MacLean, R. A. Coxall, A. R. Mount, *J. Mater. Chem.* 2000, **10**, 2043–2047.
- (44) B. Gómez-Lor, A. M. Echavarren, *Org. Lett.* 2004, **6**, 2993–2996.
- (45) E. M. García-Frutos, E. Gutierrez-Puebla, M. A. Monge, R. Ramírez, P. Andrés, A. Andrés, R. Ramírez, B. Gómez-Lor, *Org. Electron.* 2009, **10**, 643–652.
- (46) F. Wang, X.-C. Li, W.-Y. Lai, Y. Chen, W. Huang, F. Wudl, *Org. Lett.* 2014, **16**, 2942–2945
- (47) Xiangchun Li, Chunyu Wang, Yibo Xue, Cheng Meng, Prof. Wen-Yong Lai and Prof. Wei Huang, *Asian J. Org. Chem.* 2017, **6**, 1749–1754
- (48) X.-C. Li, C.-Y. Wang, W.-Y. Lai, W. Huang, *J. Mater. Chem. C*, 2016, **4**, 10574–10587
- (49) C.-F. Liu, C. Cheng, Y. Jiang, W.-Y. Lai, W. Huang, *New J. Chem.*, 2017, **41**, 13619–13624
- (50) X.-C. Li, Y. Zhang, C.-Y. Wang, Y. Wan, W.-Y. Lai, H. Pang, W. Huang, *Chem. Sci.*, 2017, **8**, 2959–2965
- (51) M. R. Maciejczyk, J. A. G. Williams, N. Robertson, M. Pietraszkiewicz, *RSC Adv.* 2017, **7**, 49532–49535
- (52) S. Mun, S. Lee, Y. Choi, B. Lee, S. Yeo, Duksan High Metal Co., Ltd. WO 2014/061960 A1, 2014.
- (53) M. Tada, M. Matsumoto, Nippon Steel Chemical Co., Ltd., WO 2012/073888 A1, 2012.
- (54) L. Chen, J. J. Baldwin, C. Wu, C. Shen, C. MGLUR Regulators. WO 2014/124560 A1, 2014.
- (55) T. A. Engler, W. Chai, *Tetrahedron Lett.* 1996, **37**, 6969–6970.
- (56) T. Bach, M. Bartels, *Synthesis* 2003, **6**, 925–939.
- (57) T.-S. Ahn, R. O. Al-Kaysi, A. M. Müller, K. M. Wentz, C. J. Bardeen, *Rev. Sci. Instrum.* 2007, **78**, 086105-(1-3)
- (58) D. Baunsgaard, M. El. Balsami, J. Frederiksen, N. Harrit, F. Negri, G. Orlandi, R. Wilbrandt, *Laser Chem.* 1999, **19**, 349–351.
- (59) N. H. Tinh, P. Foucher, C. Destrade, A. M. Levelut, J. Malthete, *Mol. Cryst. Liq. Cryst.* 1984, **111**, 277–292.
- (60) J.-L. Wang, X. Li, C. D. Shreiner, X. Lu, C. N. Moorefield, S. R. Tummalapalli, D. A. Medvetz, M. J. Panzner, F. R. Fronczek, C. Wesdemiotis, G. R. Newkome, *New J. Chem.* 2012, **36**, 484–491.



5-oxatruxene presents new quality among truxenes. It is promising compound for the new class of optoelectronic materials.